Zipeng Guo
Department of Industrial and Systems Engineering, University at Buffalo, The State University of New York, Buffalo, NY 14260
e-mail: zipenggu@buffalo.edu

Ruizhe Yang
Department of Mechanical and Aerospace Engineering, University at Buffalo, The State University of New York, Buffalo, NY 14260
e-mail: ruizheya@buffalo.edu

Tianjiao Wang
Department of Industrial and Systems Engineering, University at Buffalo, The State University of New York, Buffalo, NY 14260
e-mail: twang38@buffalo.edu

Lu An
Department of Mechanical and Aerospace Engineering, University at Buffalo, The State University of New York, Buffalo, NY 14260
e-mail: luan@buffalo.edu

Shenqiang Ren
Professor
Department of Mechanical and Aerospace Engineering, Department of Chemistry, University at Buffalo, The State University of New York, Buffalo, NY 14260
e-mail: shenren@buffalo.edu

Chi Zhou[1]
Associate Professor
Department of Industrial and Systems Engineering, University at Buffalo, The State University of New York, Buffalo, NY 14260
e-mail: chizhou@buffalo.edu

Cost-Effective Additive Manufacturing of Ambient Pressure-Dried Silica Aerogel

The conventional manufacturing processes for aerogel insulation materials mostly rely on the supercritical drying, which suffers from issues of massive energy consumption, high-cost equipment, and prolonged processing time. Considering the large market demand for the aerogel insulation material in the next decade, a cost-effective and scalable fabrication technique is highly desired. In this paper, a direct ink writing (DIW) method is used to three-dimensionally fabricate the silica aerogel insulation material, followed by room-temperature and ambient pressure drying. Compared with the supercritical drying and freeze-drying techniques, the reported method significantly reduces the fabrication time and costs. The cost-effective DIW technique offers the capability to print complex hollow internal structures, coupled with the porous aerogel structure, it is found to be beneficial for the thermal insulation property. The addition of fiber to the ink assures the durability of the fabricated product, without sacrificing the thermal insulation performance. The foam ink preparation methods and the printability are demonstrated in this paper, along with the printing of complex three-dimensional geometries. The thermal insulation performance of the printed objects is characterized, and the mechanical properties were also examined. The proposed approach is found to have a 56% reduction in the processing time. The printed silica aerogels exhibit a low thermal conductivity of 0.053 W m^{-1} K^{-1}.
[DOI: 10.1115/1.4048740]

Keywords: additive manufacturing, 3D printing, silica aerogel, ambient pressure drying

1 Introduction

Aerogel as a multiscale solid structure with ultra-high porosity and low density is a preferable material for thermal insulation purposes. Aerogel has strategical importance in wide-spreading applications, including construction and architecture [1,2], aerospace and automobile [3], energy conversion and storage industries [4], etc. Among various thermal insulation materials, silica aerogels exhibit the lowest thermal conductivity when compared with any other structures known so far, at a level of 0.015 W/m·K at ambient temperature [5]. The commercially available aerogel products from Aspen [6,7] and Cabot [8] offer thin (5–10 mm thickness), hydrophobic, sound-proof, and flexible aerogel insulation sheets. These products are synthesized by the approach of supercritical condition drying [9]. The supercritical drying is a common approach to fabricate aerogels by removing the low surface tension liquid from the silica skeletons, with the help of supercritical CO_2 or CH_4 to produce crack-free aerogel. Due to the prohibitively expensive equipment and time costs, aerogel production remains largely limited on an industrial scale. It is anticipated to cost $7.2 to produce one square-meter of silica aerogel sheet (3 cm thick) [10]. Furthermore, the drying cost increases exponentially with the increasing thickness of the sheet.

Alternative approaches to fabricate aerogel include freeze-drying and ambient pressure drying (APD). Although the freeze-drying lowers down the fabrication cost, it suffers from scalability issues,

[1]Corresponding author.

Manuscript received May 20, 2020; final manuscript received September 22, 2020; published online December 3, 2020. Assoc. Editor: Sam Anand.

including high-cost, low-efficiency, and small-dimension. The conventional ambient pressure drying process is a less energy-intensive approach. The organic solvents are used in the precursor gel, such as hexane, heptane, and octane. Due to their low surface tension during the ambient drying process, this method is also applicable for fabricating crack-free aerogels. However, it usually leads to the generation of hydrochloric acid, which needs to be further removed by other organic solvents [11,12]. The use of a large amount of organic solvents poses challenges for large-scale production and real-world applications.

Researchers have also explored the additive manufacturing or 3D printing, as an advanced manufacturing technique to fabricate complex-structure objects, and print aerogels with porous structures. Inspired by the unique layer-by-layer fabrication concept, 3D printing is capable of manipulating the hierarchical structure both internally and externally. The 3D printing techniques bring huge potential to produce highly customized aerogel products with intricate macroscale architecture and microscale structure at the same time. Among various 3D printing processes, the drop-on-demand inkjet printing has been used to print graphene oxide ink into a truss structure and also print ice to support the bridges above the hollow regions. The building environment has a temperature well below the freezing point [12–18]. The printed ice will be further removed by the freeze-drying process, leaving an ultra-low-density graphene oxide network. In this case, the freeze-drying serves as an indirect way to produce the internal porous structure.

The direct ink writing (DIW) has been used to fabricate hybrid silica aerogel [19], the hybrid silica aerogel was made by assembling the silk fibroin biopolymers inside the silica structure to make the structure flexible and fire retardant. The prepared ink shows good printability and the direct ink writing can print parts with customized morphology and microstructures. After printing, the sample was put into an oven for the sol-gel reaction/gelation and finally dried using the supercritical CO_2 drying. Other researchers have been trying direct ways to generate the porous structure. Toward direct printing a hierarchical cellular structure with low-density and high-porosity structure, a direct foam writing technology was reported by Muth et al. [20]. A viscoelastic foamed ink was designed, the air bubbles inside the ink formed a bubble microstructure and retained the bubble characteristic content and size over a long period of time. The printed specimen was sintered to fabricate high-porosity structures. Compared with the inkjet printing technique, this approach can achieve scalable fabrication of porous materials and has large potential applications in thermal insulation. However, the bubbles in the ink were introduced only by vigorously stirring; therefore, the bubbles cannot stably stay inside the ink due to their low surface tension. Over time, small bubbles could merge together and eventually float up and accumulate at the top surface. Moreover, the printed sample undergoes a set of sophisticated and time-consuming drying procedures. Despite the fact that these methods were capable of fabricating porous and mechanically strong aerogels, the processing time is a vital bottleneck for producing large-scale aerogels.

Taking advantage of printing complex internal structures in three-dimensional space, 3D printing could save the material by designing the hollow internal structure and tuning the infill density. Coupled with ambient pressure drying, which can in-situ generate the porous structure, the integrated process has the potential to scale up the manufacturing process by significantly reducing the monetary cost and time cost. In this regard, we propose to combine the direct ink writing and ambient pressure drying to 3D print silica aerogel insulation material. While it is challenging to have good thermal insulation behavior as well as maintain the mechanically strong property for the high-porosity structure. Herein, a direct ink writing technique combined with an ambient pressure drying approach is demonstrated as a cost-effective production method. The innovation of this approach is the cost-effective in-situ porous generation process and the durable pore-supporting structure facilitated by various additives, including the foaming agent and fiber. With the assistant of a foaming agent, the surface tension between the ink and the gaseous bubbles can be lowered, such that bubbles can be stably distributed inside the aerogel ink [21]. Two types of foaming agents are widely used, the cationic cetyltrimethylammonium bromide (CTAB) [22,23] and the anionic sodium dodecyl sulfate (SDS) [24]. With the pressure in the resulting bubbles is opposing to the capillary pressure, it prevents the pore shrinkage or collapse during the ambient pressure drying process. Compared to the supercritical point drying, where the pores were produced by removing the solvent using the precise and expensive equipment, our reported ambient pressure and temperature drying approach can significantly reduce the energy, time, and equipment cost. To facilitate the printing in three-dimensional (3D) space with customized structure, the 3D printable ink with embedded gaseous bubbles was designed. Based on the precursor, a few additives were added to modify the rheological properties of the ink. Specifically, the cellulose-based viscosity modifier can make the ink viscous enough to gain a shear-thinning behavior. The highly viscous and shear-thinning non-Newtonian fluid is preferable for printing high-quality specimens. Fiber was added to the ink to reinforce the mechanical strength. As shown in Figs. 1(*a*) and 1(*b*), the diagram illustrates the procedures of preparing the printable ink, two-step blending was required. The premixing of the precursor was aimed to distribute the solid particles uniformly in the solvent. Then, the foaming agent was added and followed by vigorously blending to generate gaseous bubbles in the ink.

Figure 1(*c*) is a schematic drawing to demonstrate the printing process. With the applied downward mechanical force, the ink was extruded and printed to the 3D structure. Different 3D structures are printed to demonstrate the printability. Figure 1(*d*) is the aerogel printed logo of the University at Buffalo (UB). As introduced, after printing the UB logo, it was dried in an ambient pressure and temperature environment.

The remainder of this paper is organized as follows: in Sec. 2, the printable ink preparation, printing process, and drying methods are introduced; the printability of the prepared ink is also discussed. In Sec. 3, several 3D printed objects with complex geometries are shown, and their thermal insulation performances are presented. Section 4 demonstrates a comparison of drying methods to verify the cost-effectiveness of the proposed ambient pressure drying process. The characterization results of thermal insulation property and mechanical property are illustrated. Section 5 is a comprehensive discussion of the results. Conclusion and future works are presented in Sec. 6.

2 Materials and Methods

2.1 Printable Ink Preparation. The printable ink in general shall exhibit the rheological behavior with highly viscous and shear-thinning properties. The ink preparation is critical for ensuring the printing quality. First, the ink was prepared by mixing TEOS-based aerogel powder into the solvent at a concentration of 60wt%. The solvent was made by dissolving polyvinyl alcohol (PVA, Mw ~ 10,000; Sigma-Aldrich, St. Louis, MO) into deionized (DI) water at a concentration of 0.05 g/mL of the DI water. PVA serves as the binder to improve the strength and integrity of the printed sample. The good integrity also makes the printed sample less dusty after drying. Darvan 811(Vanderbilt Minerals, Norwalk, CT) was added by 1.6 vol% of the DI water to disperse the aerogel powders. The commercially available Fiber sheet (E08, Unifrax, Buffalo, NY) was blended using a food blender (BBR-2001; Capbran Holdings, Los Angeles, CA), then added to the prepared solvent by 10 wt% of the aerogel powder. The suspension was then pre-mixed homogenously for 6 h on a magnetic stirring hot plate (UX-04600-12; Thermo Scientific, Waltham, MA). Hereafter, hydroxypropyl methyl cellulose (HPMC, H7509; Sigma-Aldrich, St. Louis, MO) was added to the suspension as a viscosity modifier at a concentration of 12 mg/mL of the DI

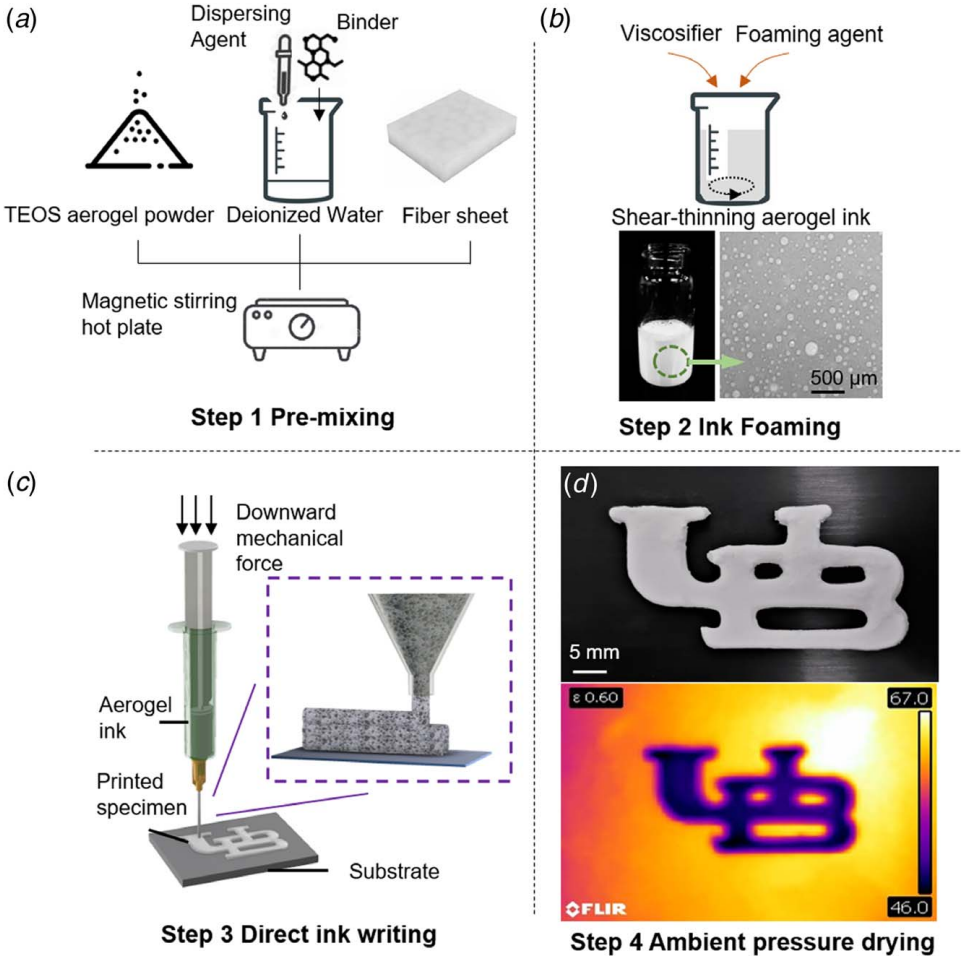

Fig. 1 Direct ink writing of silica aerogel insulation material. (*a*) The recipe and pre-mixing step of preparing aerogel ink. (*b*) The presence of additives in the ink ensures its printability. The gaseous bubbles are uniformly distributed in the ink. (*c*) Schematic diagram of the direct ink writing process. (*d*) The aerogel printed object with a UB logo geometry and its infrared image showing the thermal insulation property.

water. HPMC was equally split into two batches, adding to the suspension sequentially. The first batch was added and followed by blending for 3 h, then the second batch was added and also blended for 3 h. Sequentially adding the HPMC will help it to be thoroughly dissolved into the suspension, whereas directly adding the entire batch will cause HPMC to tangle together and makes the ink difficult to blend. Finally, CTAB (VWR, Radnor, PA) was added as the surfactant to form uniformly distributed gaseous bubbles, which will be developed into the porous structure after printing [25–27]. Unlike the conventional way to make printable ink, where a defoamer-like chemical such as 1-Octanol is added to make smooth and continuous paste (slurry) [28,29], the proposed approach in this work took the opposite route by adding a foaming agent to generate the pore-supporting porous structure. Although with the presence of defoamer, the printed sample using conventional approach will have good integrity, but essentially resulted in a dense structure, which is not ideal for thermal insulation purposes. By vigorously blending the ink, the foaming agent generated abundant gaseous bubbles in the ink. The bubbles can retain the size and quantity after 1 week of aging in a closed container. Figure 1(*b*) shows the ready-to-print ink, the sub-figure is a close-up view of the ink and the gaseous bubbles were evenly distributed in the ink.

2.2 Direct Writing of Silica Aerogel Ink. A custom-built 3D printer was constructed; the screw-driven linear stage (Velmex XN10, Bloomfield, NY) was mounted onto the printer; and this linear stage provides a mechanical force for extruding the aerogel ink. As the stage moved down, a downward mechanical force will be generated, which then exerted on the piston of the syringe, pushing it downwards, and extruding the ink out of the nozzle. The prepared ink was loaded into a 30 mL syringe with a helix-locked conical shape nozzle (Nordson EFD, East Providence, RI) attached to the tip of the syringe. The extruder path and G-code were generated by SLIC3R software,[2] the infill pattern was set as rectilinear, and the layer thickness was 0.8 mm. As a process parameter that can only pertain to the 3D printing process, the infill density was set at 50%, 75%, and 100%, respectively, which was used to study its influence on the thermal conductivity. A stainless-steel woven mesh-sheet (SATINIOR-Woven-02) was used as a substrate, its fine meshes on the thin sheet were permeable to air. It prevented the printed sample from cracking caused by non-uniform drying. In addition, the flexible mesh sheet can be easily peeled off from the sample without damaging the bottom surface.

To achieve a continuous and stable extrusion of the ink, the effective printing speed (v_{eff}) was calculated by [20]

$$v_{eff} = \frac{Q}{\pi(d/2)^2} \tag{1}$$

where Q is the volumetric flow rate, which was measured as 9.05 mm^3/s, d is the nozzle inner diameter, a 1 mm diameter

[2] slic3r.org

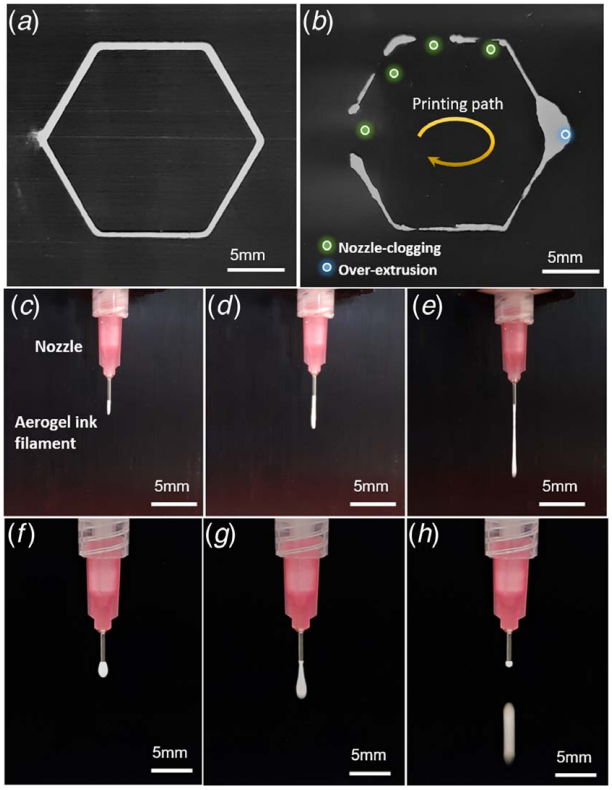

Fig. 2 Characterization of the aerogel ink. (*a*) A hexagon contour written by aerogel ink with suitable rheology. (*b*) Unfavorable ink printability. (c)–(e) The shear-thinning behavior of the aerogel ink. (*f*)–(*h*) The ink without shear-thinning behavior cannot form continuous and uniform filament.

nozzle was used to print all the samples for characterization, which corresponded to an effective printing speed of 8 mm/s. Faster printing speed will result in non-continuous filament extrusion, while an over-slow speed will cause over-extrusion.

2.3 Ambient Pressure and Temperature Drying. Once printed, the samples were dried in an ambient pressure and room temperature environment. After 6-h drying, the mesh substrate can be easily peeled off from the sample. With additional 4-h drying, the as-printed solid sample was obtained.

3 Direct-Ink-Writing of Centimeter-Scaled Three-Dimensional Complex Geometries

3.1 Printability of the Silica Aerogel Ink. The printable ink shall be shear-thinning non-Newtonian fluid with a high viscosity. The shear-thinning behavior is essential to facilitate the DIW method, because it ensures that the filament can readily and continuously flow through the nozzle under shear through the nozzle. The highly viscous ink enables the printed aerogel objects to maintain a free-standing and three-dimensional structure by a sufficiently high yield stress and storage modulus. Figure 2 shows a qualitative characterization of the ink. Figure 2(*a*) is a hexagon shape contour, which was printed using the typical printable aerogel ink, where the filament can be uniformly extruded from the nozzle. If the aerogel or the fiber is not uniformly distributed in the ink, it could cause the nozzle-clogging issue, as shown in Fig. 2(*b*), where the nozzle-clogging and over-extrusion issues were observed, indicating an unfavorable ink printability. Whenever the nozzle-clogging happens, it causes an undesirable accumulation of the extrusion pressure. As a result, it leads to subsequent over-extrusion. Figures 2(*c*)–2(*e*) are the sequential photographs showing the shear-thinning behavior of the printable ink. Compared with Figs. 2(*f*)–2(*h*), where the ink did not possess a shear-thinning property, and no continuous or uniform filaments were formed. Upon extrusion, the ink first accumulated at the nozzle tip and form the drop-like shape, it subsequently dripped down under its own gravity.

3.2 Direct-Ink-Writing of Silica Aerogel. Figure 1(*d*) shows an infrared (IR) image as a demonstration of the thermal insulation property of the printed UB logo. The image was captured after 30 min of heating. The base-plate temperature was 67 °C, and the top surface of the UB logo was 46 °C. The temperature difference between the heat plate and the top surface of the logo shows effective thermal insulation, and the uniform color on the logo IR image shows good integrity of the printed specimen.

To further validate that the proposed technique is capable of printing silica aerogel material in free-standing, three-dimensional structure with high resolution, several CAD models were first built, namely (1) twist cylinder model, (2) high-aspect-ratio wavy vase model, (3) short curvy vase model, (4) tall vase model, and (5) oval bowl model. The CAD models were then sliced, and its G-code was generated accordingly. The parameter settings are listed in Table 1. Figure 3(*b*1) shows the printed silica aerogel parts.

(1) Twist cylinder model: A solid infilled printed object, with the twisted contour in the vertical direction.
(2) High-aspect-ratio wavy vase model: A hollow object with 70:1 aspect-ratio. With the relatively extreme thin wall, the object stands well in its as-printed shape.
(3) Short curvy vase model: With a small layer thickness and nozzle size, the curvy shape contour can be printed in high resolution.
(4) Tall vase model: A tall and hollow structure shows the rheology of aerogel ink was quite suitable for direct ink printing, so that the complex geometries can be clearly printed.
(5) Oval bowl model: The printed object shows very uniform layers, indicating the extrusion was very smooth and uniform. Since the model has a higher dimension, relatively large layer thickness and nozzle size were adopted to print this model to save the printing time.

3.3 Thermal Insulation Performance of the Printed Objects. After the 3D objects were printed, its thermal insulation

Table 1 Parameter settings for direct-ink-writing process

Object name	Dimension ($L \times W \times H$, mm)	Printing time (min)	Nozzle size (mm)	Layer thickness (mm)	Infill
Twist cylinder	10 × 10 × 22	40	0.40	0.3	Solid
High-aspect-ratio wavy vase	12 × 12 × 36	35	0.40	0.3	Hollow
Short curvy vase	14 × 14 × 22	13	0.40	0.25	Hollow
Tall vase	28 × 28 × 42	45	0.50	0.35	Hollow
Oval bowl	30 × 30 × 30	25	0.50	0.35	Hollow

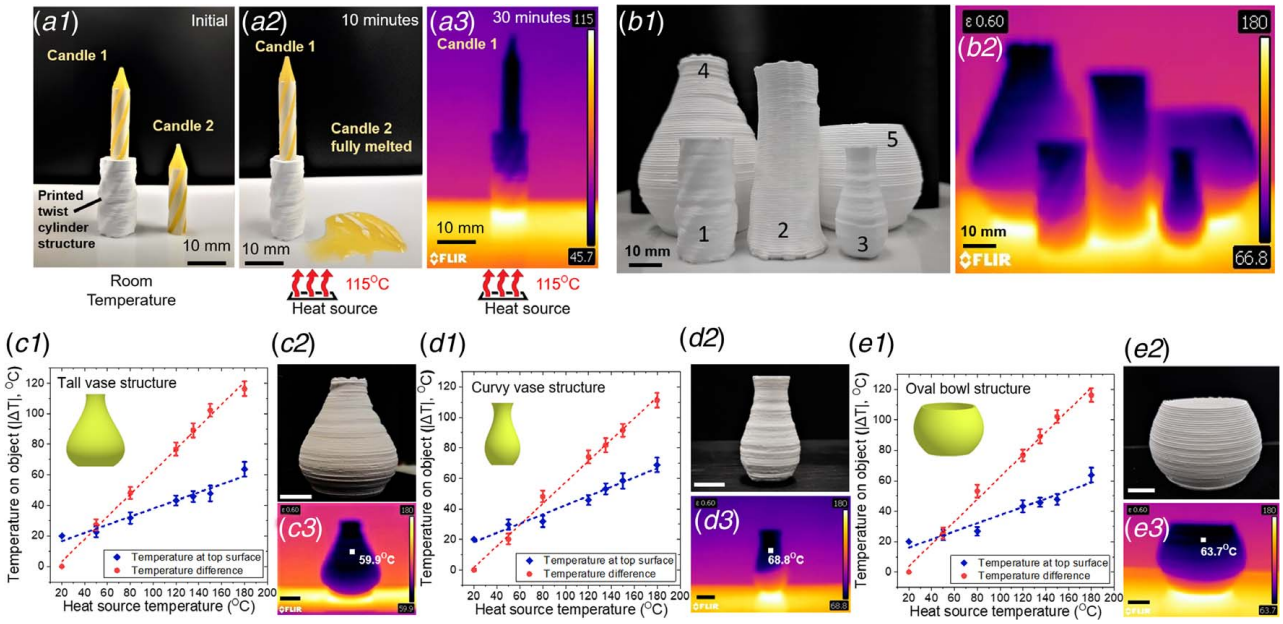

Fig. 3 Thermal insulation demonstration of the 3D printed aerogel objects. (*a*1)–(*a*3) The candle demonstration. The candle 1 was placed on the 3D printed twist cylinder and stayed intact, candle 2 was placed directly on the heat plate, it was melted after 10 min heating. (*b*1) shows the printed aerogel objects with three-dimensional complex geometries, namely 1. Twist cylinder model; 2. High-aspect-ratio wavy vase model; 3. Short curvy vase model; 4. Tall vase model; 5. Oval bowl model. (*b*2) shows the IR image of all the printed objected, with the heat source set at 180 °C, the lowest temperature on the object is 66.8 °C. (c1)–(c3) Temperature profile on the printed tall vase model, and the temperature difference between the object and heat source. The heat source was set at 180 °C. (*d*1)–(*d*3) Temperature profile on the printed short curvy model, and the temperature difference between the object and heat source. (e1)–(e3) Temperature profile on the printed tall vase model, and the temperature difference between the object and heat source. All the scale bars represent 10 mm.

performance was examined. Two demonstrations were conducted, the first one is a candle demonstration, as shown in Figs. 3(*a*1)–3(*a*3). Two identical candles were prepared, with one positioned directly on the heat plate, the other one sits on top of the printed twist cylinder part (printed part 1). The hypothesis is the aerogel sample will prevent the heat from penetrating into the candle, so that the candle stays intact. While the other candle will be quickly melted due to the heat. The demonstration starts from room temperature, then the heat plate temperature was set at 115 °C. After 5 min of heating, the bottom of candle 2 began to melt and then fall down, while candle 1 kept the original shape. After heating for 10 min, candle 2 was fully melted, as shown in Fig. 3(*a*2), candle 1 still stayed intact. Finally, an IR image was taken after 30 min of heating, and it can be seen from the IR image that the printed twist cylinder part insulated the majority of the heat from the bottom, preventing the candle 1 from melting. With the heat source increasing from room temperature to 115 °C, the candle 1 body temperature increased only to 45.7 °C, which means 75.3% of the temperature increase was insulated by the aerogel printed object.

Figures 3(*b*1) and 3(*b*2) show the set of 3D printed objects, along with the IR image, where the heat source temperature was set at 120 °C, 130 °C, 150 °C, and 180 °C, respectively. The lowest temperature on each object body is summarized in Table 2. The hypothesis is that regardless of the object geometry, all the printed samples should have the same level of the thermal insulation property. In Table 2, the heat insulation rate refers to the ratio of temperature increase (ΔT_O) of the object to the temperature increase (ΔT_H) of the heat source. At different heat source temperatures, the printed object has a near-identical heat insulation rate, at a level of 73%, which indicates its thermal insulation behavior is independent of the temperature change. The 3D printed aerogel objects can achieve the same thermal insulation performance, regardless of the geometry and the environment temperature.

The thermal insulation behavior of the printed objects under different heat source conditions was also observed. The temperature change on the object body along with the absolute temperature difference ($|\Delta T|$) of the object and the heat plate were plotted versus the heat plate temperature. The heat source temperature was set at 50 °C, 80 °C, 120 °C, 135 °C, 150 °C and 180 °C, respectively. Three experiments were performed separately, the printed parts and IR images were shown in Figs. 3(*c*1)–3(*e*3). As shown in the plots, the temperature-difference increases linearly as increase in the heating-source temperature, indicating a better thermal insulation performance at a higher temperature. The linearity was observed over all the objects, which verifies the hypothesis that the thermal insulation property of the printed aerogel specimen is independent of the geometries.

Table 2 Temperature profile on the printed object

Heat source temperature	Lowest temperature on object	Temperature difference	Heat insulation rate
120 °C	49.6 °C	70.4 °C	72.58%
130 °C	51.8 °C	78.2 °C	73.07%
150 °C	56.3 °C	93.2 °C	73.38%
180 °C	65.8 °C	114.2 °C	72.74%

4 Characterizations and Experimental Results

The following characterization and experimental study are first performed to study the thermal insulation behavior with respect to different drying methods, namely, freeze-drying, sintering, and ambient pressure drying. It is aimed to demonstrate the ambient pressure and temperature drying can result in the same level of thermal conductivity performance while it can substantially reduce the drying process time and cost. Then, the infill density,

fiber concentration, and foaming agent concentration, as three of the major process parameters, were studied, respectively, which can provide a guidance on the optimization of the printing process, aiming to reach an optimum pore size control and thermal insulation property. Finally, the compression tests were performed for the direct-ink-printed, crack-free samples to characterize the mechanical property.

4.1 Drying Methods Comparison. To verify the ambient pressure drying is a cost-effective drying method for producing the high porosity silica aerogel insulation material, three different drying methods were compared, namely, freeze-drying, sintering, and ambient pressure drying. The sample for this set of tests was cubic shapes with a dimension of 30 mm in length by 30 mm in width by 8 mm in thickness.

To perform the freeze-drying method, the printed cubic samples were first frozen in a refrigerator at −20 °C. The freeze-drying system (FreeZone Triad Model 7400 Series; LABCONCO, Kansas City, MO) was pre-frozen to −40 °C, then the sample was put into the chamber. The primary drying process started from −40 °C, ramped to −10 °C at a rate of 0.25 °C/min and held at −10 °C for 6 h. Followed by the secondary drying process started from −10 °C, warm up to 0 °C at a rate of 0.25 °C/min, and held at 0 °C for 6 h. Finally, the chamber temperature was elevated to 20 °C at the rate of 0.25 °C/min and hold for 2 h, to allow the solvent content to be completely sublimated. The vacuum of the system was maintained at 0.013–0.018 mBar during the entire drying process. The processing time was 23 h in total.

The sintering method aims to burn out the organic component inside the sample, left with the empty pore structure. The printed sample was first dried at room temperature for 6 h, after the substrate was removed from the sample, then transferred into a tube furnace (GSL-1500X; MTI Corporation, Richmond, CA). The heating profile began from room temperature, then ramped up to 400 °C at a rate of 2 °C/min and holds for 2 h at 400 °C, followed by natural cooling to room temperature. The processing time was 13 h in total.

As described in Sec. 2.4, the room-temperature ambient pressure drying took 10 h in total. After the samples were dried using three different methods, the thermal conductivity was measured by a custom-built heat flux sensing instrument. It was composed of a heated plate at the top and a cooled plate at the bottom, with two heat flux sensors attached to each plate. The temperature of the heated plate remained constant at 37 °C, and the temperature of the cooled plate was set at 30 °C. The sample was placed in between the two heat flux sensors. The heat flux and thermal conductivity relationship is given by

$$q = \frac{-\lambda * \Delta T}{\Delta x} \tag{2}$$

where q is the heat flux value collected by the sensors, λ is the thermal conductivity, ΔT is the temperature difference across the sample collected by the embedded thermal couple in the sensors, and Δx refers to the thickness of the sample. In general, the negative sign is an indication of the direction of the heat transfer.

The results are shown in Fig. 4(*a*), it confirms the hypothesis that three different drying methods reach the same level of thermal insulation performance, with the ambient pressure and temperature drying has the lowest thermal conductivity, and the freeze-drying has the highest thermal conductivity. Further considering the processing time, freeze-drying takes more than twice the time compared with the ambient pressure drying. It is sufficient to conclude that ambient pressure drying is effective for 3D printing of silica aerogel insulation material at low cost.

4.2 Density Measurements. The sample density was calculated according to the mass and volume of the samples. Mass was measured by using a weighing scale (AX223, OHAUS, Parsippany, NJ). The sample volume was measured with the gas-replacement pycnometer (Micromeritics Accu-Pyc II 1340, Norcross, GA). Three sets of samples were compared, one set was the dense samples, where no foaming agent was included in the ink recipe, resulting in very limited pores in the sample. In comparison, the other two sets of samples were considered as porous samples, where the cetyltrimethylammonium bromide (CTAB) and SDS acting as the foaming agents were added at a concentration of 0.5 wt% of the aerogel powder. The foaming agent generates gaseous bubbles in the ink, which will be further developed into the porous structures. As shown in Fig. 4(*b*), the sample density against the different infill density was plotted. With the presence of a foaming agent, the density of the porous samples was reduced to one-third of the dense samples, indicating the foaming agent plays a vital role in generating the porous structures.

4.3 Thermal Conductivity Measurements. Thermal conductivity is one of the key factors for the thermal insulating property. Three sets of experiments were studied to investigate the relation between the process parameter and the thermal conductivity, namely, the infill density, the foaming agent concentration, and the fiber concentration.

4.3.1 Study the Influence of Infill Density on the Thermal Conductivity. The infill density describes the amount of ink printed inside the object, which can be precisely designed and controlled in additive manufacturing. Less infill density results in saving material and increasing the printing efficiency. Three infill-densities were compared, 50%, 75%, and 100%, respectively. The result is shown in Fig. 4(*c*), the fully filled sample has the highest thermal conductivity, while the 50% infill samples reach the lowest thermal conductivity with a 20% reduction. The same trends were observed for both CTAB- and SDS-foamed samples. The result concludes that relatively less infill density benefits the thermal insulation property. Consider a 50% infilled sample, the other 50% was left as empty pores, and the pattern was precisely controlled by the printing process, together with the micro-pores generated by the surfactant, which makes it less conductive to the heat.

4.3.2 Study the Influence of Foaming Agent Concentration on the Thermal Conductivity. The effect of the foaming agent concentration on the thermal conductivity was studied in order to find an optimum value to reach the best insulation performance. Two foaming agents were used, CTAB and SDS at four concentrations, 0 wt%, 0.15 wt%, 0.3 wt%, and 0.5 wt%, respectively. As indicated in Fig. 4(*d*), the dense sample has the highest thermal conductivity, while the 0.3 wt% concentration sample has the lowest value. The thermal conductivity of CTAB-foamed samples reach to 0.065 W/m*K and SDS-foamed samples reach to 0.053 W/m*K. Further increase in the concentration will result in an increase in the thermal conductivity again. It is reasonable that for the dense sample, due to the very limited pores inside the sample, the conductivity is high. With the presence of a foaming agent, the generated pores help to lower down the conductivity. While the reason that 0.5 wt% concentration sample has higher conductivity compared to the 0.3 wt% is due to the excessive foaming agent tends to over generate bubbles. The over generated small bubbles will combine together to large bubbles in an uncontrolled form, resulting in large pores inside the sample. When the heat transfers from the bottom, the air molecules carry the heat and quickly pass through the large empty pores without any resistance, then the heat is easily transferred to the top surface. The ideal pore structure would be uniformly distributed pores with controlled size and pattern [30].

4.3.3 Study the Influence of Fiber Concentration on the Thermal Conductivity. The fiber was added to the ink for the consideration of the mechanical strength of the printed sample. To verify the hypothesis that fiber reinforces the sample, but not

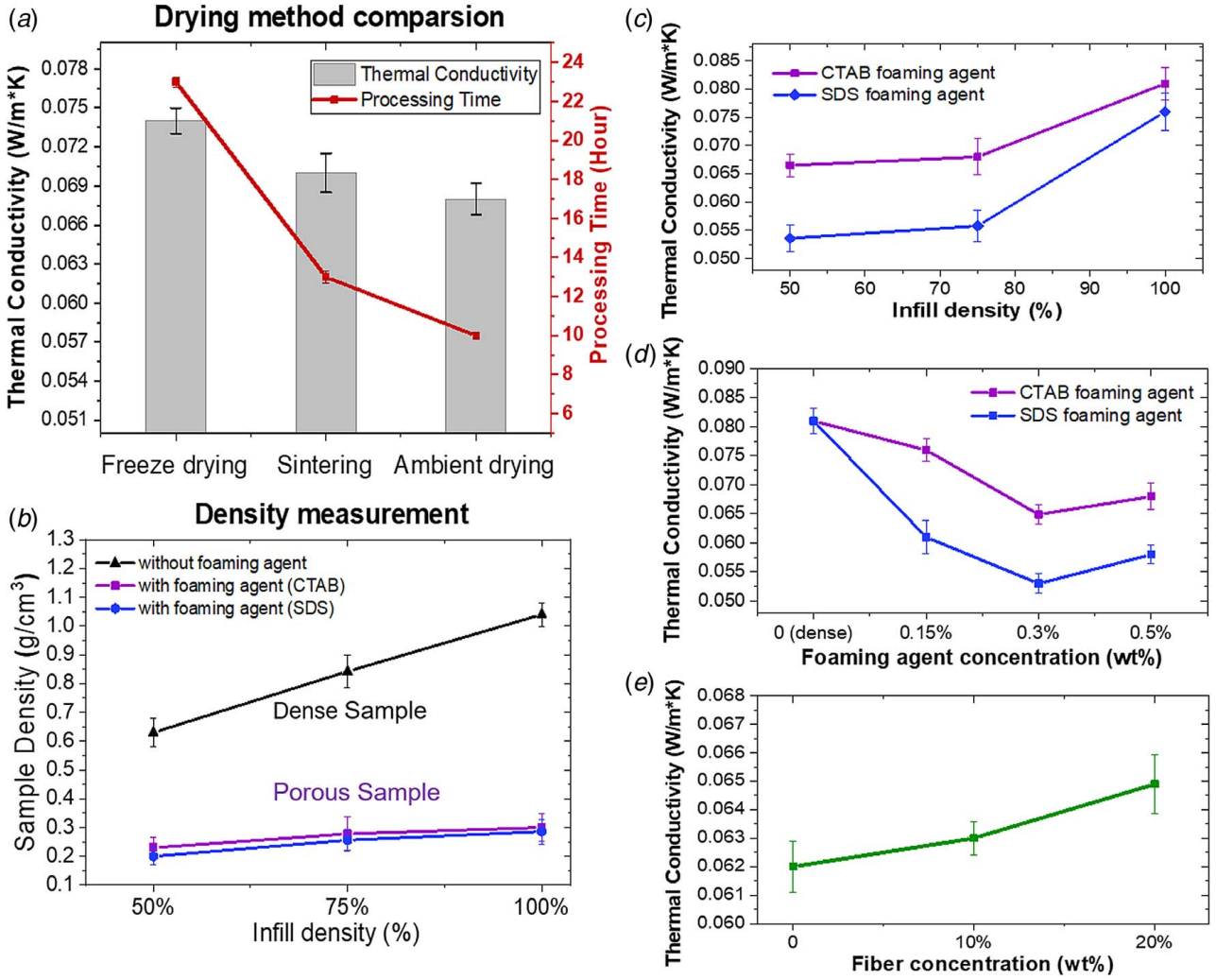

Fig. 4 The cost-effectiveness of ambient pressure drying and thermal insulation characterization results. (*a*) Comparison of freeze drying, sintering and ambient drying with respect to the thermal conductivity and processing time. (*b*) Density measurement of the printed dense and porous samples. (c) Study the influence of infill density on the thermal conductivity. (*d*) Study the influence of foaming agent concentration on the thermal conductivity. (e) Study the influence of fiber concentration on the thermal conductivity.

affects too much on the thermal conductivity, three different fiber contents were studied, 0 wt%, 10 wt%, and 20 wt%, respectively. The result is shown in Fig. 4(*e*), the change of fiber content does not cause the thermal conductivity to fluctuate too much, with a maximum value of 0.0649 W/m*K and a minimum value of 0.062 W/m*K and only a 5% deviation. While considering the mechanical strength (detailed Sec. 4.4), the addition of the fiber can significantly reinforce the sample, without affecting the insulation property.

4.4 Mechanical Characterization. The mechanical strength was characterized to show the durable pore-support structure of the printed sample, using the compression test stand (ESM303, MARK-10, Copiague, NY). As discussed in Sec. 2.3, fiber was added to the ink for printing, in order to reinforce the strength, the evaluated sample was in the cubic shape with a dimension of 10 mm long by 10 mm wide by 10 mm thick. A sample without fiber content was also characterized as a control sample.

The stress-strain curve is shown in Fig. 5(*a*), the control sample has the Young's modulus of 6.5 Mpa with a maximum load of 0.52 Mpa. While with the addition of fiber, the sample has the Young's modulus of 15.84 Mpa with a maximum load of 1.02 Mpa. Young's modulus as a mechanical property that measures the stiffness of the sample is three times stronger than without fiber content, which concludes that the fiber is effective in reinforcing the sample strength.

4.5 Characterization of the Microstructure. The microstructure of the printed sample, as illustrated in Figs. 5(*b*)–5(*e*), was characterized by scanning electron microscopy (SEM). Figure 5(*b*) shows the evenly distributed pore structures, zoomed into (*d*) demonstrates pores with combined fiber contents. Figure 5(*e*) shows the fiber bonds well with the aerogel skeleton, which substantially contributes to the increased structural strength.

5 Discussion

The experimental results from Sec. 4 are correlated to one another; here, we will comprehensively discuss all the results. Comparison of drying methods shows that the freeze-drying procedure takes the longest time, but the resulting thermal conductivity did not outperform the ambient pressure drying, meaning the time cost can be saved by 56% if using the proposed ambient pressure and temperature drying. With the consideration of expensive equipment costs of freeze-drying, the actual cost-saving is substantial. For the sintering drying method, although it is widely used for direct ink writing [31,32] to help remove all the organic solvent

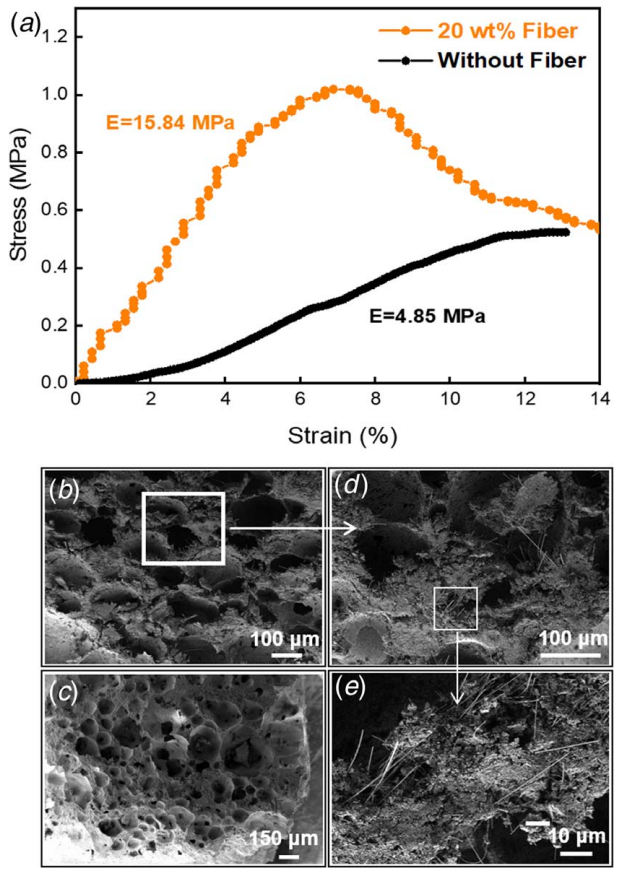

Fig. 5 Mechanical properties characterization and microstructure characterization. (*a*) Stress-Strain curves for specimens without fiber and with 20 wt% fiber content. (*b*) and (c) are SEM images to show the internal porous structure. (*d*) and (*e*) show the bonding between fiber and aerogel skeleton.

and additives, it suffers from the potential internal cracks during and after sintering, which requires adding the additives, such as binder to help prevent the structure from collapse. Furthermore, the sintering process also requires precise temperature control, which will incur considerable equipment costs. Considering manufacturing the aerogel products, neither the freeze-drying nor sintering could be an effective way. Our proposed ambient pressure and temperature drying, also result in good thermal insulation performance, but it does not require heavy equipment investment, and the processing time is significantly shorter, which makes it promising toward the large-scale and low-cost fabrication.

The ambient pressure and temperature drying (APD) largely reduced the use of organic solvents. By adding the surfactant to the aerogel ink, the surface tension between the aerogel and the solvent is reduced. As a result, the capillary pressure on the aerogel-solvent interface is dropped to a favorable level, which helps to prevent the aerogel from cracking or collapsing during the APD process. As shown in Figs. 5(*b*)–5(*d*), no cracks exhibited in the SEM images.

The mechanical strength is another important property for the aerogel products. Since aerogel has a highly porous structure, the majority of the internal structure is in the form of empty shells. Therefore, the binding of the aerogel skeleton is critical to make durable structures. Here, in order to reinforce the strength but not affect the thermal insulation performance, fiber content is added to the ink. The mechanical test shows that after adding fiber, samples have a 143% increase in Young's modulus, which indicates the fiber plays a vital role in making the sample much stiffer. The investigation of the microstructure by SEM confirms that the samples have a uniform internal porous structure and the fiber contents bind well with the skeleton. The blending procedures (Sec. 2.1) is of critical importance for good binding. Blending facilitates the relative long fiber content evenly dispersed in the ink without settling down or tangling together. It should be pointed out that after printing, the fiber is located along the longitudinal direction since the printing is done by extruding cylindrical filament and printed layer by layer. After drying, the small, scattered fiber will tangle together and form a stiff truss-like structure and therefore enhance the overall strength. On the other hand, the pore-supporting skeleton is another factor to form a durable structure. As introduced in Sec. 1, the gaseous bubbles in the ink eventually are well-developed into the pores after drying. From the SEM images in Fig. 5, no crack has been observed even at a microscale level. This concludes that the pore-supporting structure, together with the addition of the fiber content can make the printed sample strong and durable.

The process parameter study provides a guideline on how to further optimize the fabrication with respect to the thermal insulation performance. It can be concluded that with lower infill density, the sample can reach a better performance of thermal conductivity and it proved that direct ink writing is a feasible way to produce the aerogels. While 50% of infill density is the lowest reached for this study, it could be further decreased by designing the internal truss-like structures. Not only can it reach even lower infill density but also the truss-like structure is proven to be a rigid structure.

The foaming agent study shows that 0.3% concentration performs the best of thermal insulation; from Fig. 5, it is also shown that the pores were closely assembled. While with a 0.5% concentration, it performs worse than the 0.3%, primarily due to the over-generated bubbles tend to merge together to form undesired large bubbles. Also, the results show that at each concentration, SDS performs better than CTAB in terms of thermal insulating. The hydrophilic group and its charge of SDS are the deciding reason that SDS holds a better foaming ability [33]. SDS as an anionic surfactant, when it is being agitated in the ink, the charge of SDS further creates a surface charge and surface potential. The presence of surface potential promotes the electrostatic repulsion on the interface of bubble and ink; this helps to create a stable environment to maintain the bubbles in the ink [34]. While CTAB is a cationic based surfactant, which possesses a negative charge on the hydrophilic group. Although it also reduces the surface tension and very effective in creating abundant bubbles in the ink, but due to the nature of its higher nonpolar portion of the hydrophilic groups, which results in less uniformity of the bubbles [35]. Overall, with the assistance of the foaming agent, the 3D printed samples gain porous structure, which is preferable for thermal insulation materials.

For the future improvement, the better method to control of pore size can be explored from the foam ink preparation step. Based on the density of the current sample and the benchmark samples with lower thermal conductivity, they have the same level of density, which means the foaming agent content is sufficient to introduce the gaseous bubbles. However, after the bubbles are formed, a better approach of blending in order to achieve a smaller pore size shall be used to replace the current method.

6 Conclusions and Future Work

In summary, a cost-effective approach to direct-write 3D printable aerogel ink is demonstrated. The fabrication method is enabled through the development of gaseous bubbles silica aerogel ink and the direct ink writing setup. Furthermore, combined with the ambient pressure and temperature drying after printing, the samples achieve thermal insulation property and durable mechanical strength. Moreover, validation of the thermal insulation properties is observed on the 3D printed aerogel structures, the printed structure can insulate 75% of the heat. The cost-effectiveness of the proposed approach creates the potential for advanced manufacturing, experiments show the processing time can have a 56%

reduction. The future works are focused on manufacturing and large-scale production of the silica aerogel products. From the manufacturing perspective, the proposed method can be developed to fabricate customized-architecture parts for thermal insulation applications. From the large-scale production perspective, this approach can be scaled up to produce commercial insulation aerogel products.

Acknowledgment

The authors would like to gratefully acknowledge the support from the National Science Foundation (NSF) through CMMI-1846863 and U.S. Department of Energy (DOE), Office of Energy Efficiency and Renewable Energy through DEEE-0008675. We thank Dr. Mark Swihart, Dr. Jason Armstrong, Dr. Donghui Zhao, and Dr. Moein Mohammadi for the scientific discussions. The fiber sheet was kindly provided to us by Unifrax Inc.

Conflict of Interest

There are no conflicts of interest.

Data Availability Statement

The datasets generated and supporting the findings of this article are obtainable from the corresponding author upon reasonable request. The authors attest that all data for this study are included in the paper. Data provided by a third party are listed in Acknowledgment. No data, models, or codes were generated or used for this paper.

References

[1] Acharya, A., Joshi, D., and Gokhale, V. A., 2013, "AEROGEL—A Promising Building Material for Sustainable Buildings," Chemical Process Eng. Res., **9**, pp. 1–6.
[2] Riffat, S. B., and Qiu, G., 2012, "A Review of State-of-the-Art Aerogel Applications in Buildings," Int. J. Low-Carbon Technologies, **8**(1), pp. 1–6.
[3] Fesmire, J. E., 2006, "Aerogel Insulation Systems for Space Launch Applications," Cryogenics, **46**(2–3), pp. 111–117.
[4] Yang, J., Zhang, E., Li, X., Zhang, Y., Qu, J., and Yu, Z.-Z., 2016, "Cellulose/Graphene Aerogel Supported Phase Change Composites with High Thermal Conductivity and Good Shape Stability for Thermal Energy Storage," Carbon, **98**, pp. 50–57.
[5] Dorcheh, A. S., and Abbasi, M., 2008, "Silica Aerogel; Synthesis, Properties and Characterization," J. Mater. Process. Technol., **199**(1–3), pp. 10–26.
[6] Leventis, N., and Leventis, C., 2010, *Methods and Compositions for Preparing Silica Aerogels*, Google Patents.
[7] Industrial, A. A. *High Temperature Insulation—Pyrogel XTE*. 2019; Available from: https://www.aerogel.com/products-and-solutions/pyrogel-xte/default.aspx.
[8] CabotCorporation. *Aerogel Products*. 2019; Available from: http://www.cabotcorp.com/solutions/products-plus/aerogel.
[9] Aerogel.org. *Strong and Flexible Aerogels*. 2018; Available from: http://www.aerogel.org/?p=1058.
[10] Van Bommel, M., and De Haan, A., 1995, "Drying of Silica Aerogel With Supercritical Carbon Dioxide," J. Non-Cryst. Solids, **186**, pp. 78–82.
[11] Guo, X., Shan, J., Lei, W., Ding, R., Zhang, Y., and Yang, H., 2019, "Facile Synthesis of Methylsilsesquioxane Aerogels with Uniform Mesopores by Microwave Drying," Polymers, **11**(2), p. 375.
[12] Hu, W., Li, M., Chen, W., Zhang, N., Li, B., Wang, M., and Zhao, Z., 2016, "Preparation of Hydrophobic Silica Aerogel with Kaolin Dried at Ambient Pressure," Colloids Surf., A, **501**, pp. 83–91.
[13] Yang, F., Zhao, G., Zhou, C., and Lin, D., 2018, "Phase Change Materials (PCM) Based Cold Source for Selective Freezing 3D Printing of Porous Materials," Int. J. Adv. Manuf. Technol., **95**(5–8), pp. 2145–2155.
[14] Zhao, G., Lin, D., Zhou, C., 2017, "Thermal Analysis of Directional Freezing Based Graphene Aerogel Three-Dimensional Printing Process," ASME J. Micro Nano-Manuf., **5**(1), p. 011006.
[15] Zhao, G., Zhou, C., Lin, D. , 2018, "Tool Path Planning for Directional Freezing-Based Three-Dimensional Printing of Nanomaterials," ASME J. Micro Nano-Manuf., **6**(1), p. 010905.
[16] Zhang, F., Yang, F., Lin, D., Zhou, C., 2017, "Parameter Study of Three-Dimensional Printing Graphene Oxide Based on Directional Freezing," ASME J. Manuf. Sci. Eng., **139**(3), p. 031016.
[17] Yan, P., Brown, E., Su, Q., Li, J., Wang, J., Xu, C., Zhou, C., and Lin, D., 2017, "3D Printing Hierarchical Silver Nanowire Aerogel with Highly Compressive Resilience and Tensile Elongation Through Tunable Poisson's Ratio," Small, **13**(38), p. 1701756.
[18] Zhang, Q., Zhang, F., Medarametla, S. P., Li, H., Zhou, C., and Lin, D., 2016, "3D Printing of Graphene Aerogels," Small, **12**(13), pp. 1702–1708.
[19] Maleki, H., Montes, S., Hayati-Roodbari, N., Putz, F., and Huesing, N., 2018, "Compressible, Thermally Insulating, and Fire Retardant Aerogels Through Self-Assembling Silk Fibroin Biopolymers Inside a Silica Structure—An Approach Towards 3D Printing of Aerogels," ACS Appl. Mater. Interfaces, **10**(26), pp. 22718–22730.
[20] Muth, J. T., Dixon, P. G., Woish, L., Gibson, L. J., and Lewis, J. A., 2017, "Architected Cellular Ceramics with Tailored Stiffness via Direct Foam Writing," Proc. Natl. Acad. Sci. U. S. A., **114**(8), pp. 1832–1837.
[21] Kartashynska, E., Lylyk, S., Aksenenko, E., Makievski, A., Vysotsky, Y. B., Fainerman, V., and Miller, R., 2020, "Surface Tension at the Interface Between Aqueous Solution of Surfactant and Alkane. A Comprehensive Quantum Chemical and Thermodynamic Approach," Colloids Surf., A, **591**, p. 124557.
[22] Zhang, S., Lan, Q., Liu, Q., Xu, J., and Sun, D., 2008, "Aqueous Foams Stabilized by Laponite and CTAB," Colloids Surf., A, **317**(1–3), pp. 406–413.
[23] Gao, G., Xiang, Y., Lu, S., Dong, B., Chen, S., Shi, L., Wang, Y., Wu, H., Li, Z., and Abdelkader, A., 2018, "CTAB-assisted Growth of Self-Supported Zn 2 GeO 4 Nanosheet Network on a Conductive Foam as a Binder-Free Electrode for Long-Life Lithium-ion Batteries," Nanoscale, **10**(3), pp. 921–929.
[24] Yekeen, N., Manan, M. A., Idris, A. K., and Samin, A. M., 2017, "Influence of Surfactant and Electrolyte Concentrations on Surfactant Adsorption and Foaming Characteristics," J. Pet. Sci. Eng., **149**, pp. 612–622.
[25] Yang, R., Hu, F., An, L., Armstrong, J. N., Hu, Y., Li, C., Huang, Y., and Ren, S., 2019, "A Hierarchical Mesoporous Insulation Ceramic," Nano Lett., **20**(2), pp. 1110–1116.
[26] An, L., Wang, J., Petit, D., Armstrong, J. N., Hanson, K., Hamilton, J., Souza, M., Zhao, D., Li, C., and Liu, Y., 2020, "An all-Ceramic, Anisotropic, and Flexible Aerogel Insulation Material," Nano Lett., **20**(5).
[27] Yang, R., Wang, J., An, L., Petit, D., Armstrong, J. N., Liu, Y., Huang, Y., Hu, Y., Shao, Z., and Ren, S., 2020, "A Macromolecular Assembly Directed Ceramic Aerogel Monolith Material," J. Mater. Chem. C, **8**(30), pp. 10319–10324.
[28] M'barki, A., Bocquet, L., and Stevenson, A., 2017, "Linking Rheology and Printability for Dense and Strong Ceramics by Direct ink Writing," Sci. Rep., **7**(1), p. 6017.
[29] Song, X., Tetik, H., Jirakittsonthon, T., Parandoush, P., Yang, G., Lee, D., Ryu, S., Lei, S., Weiss, M. L., and Lin, D., 2019, "Biomimetic 3D Printing of Hierarchical and Interconnected Porous Hydroxyapatite Structures With High Mechanical Strength for Bone Cell Culture," Adv. Eng. Mater., **21**(1), p. 1800678.
[30] Liu, J., Li, Y., Li, Y., Sang, S., and Li, S., 2016, "Effects of Pore Structure on Thermal Conductivity and Strength of Alumina Porous Ceramics Using Carbon Black as Pore-Forming Agent," Ceram. Int., **42**(7), pp. 8221–8228.
[31] Nan, B., Olhero, S., Pinho, R., Vilarinho, P. M., Button, T. W., and Ferreira, J. M., 2019, "Direct ink Writing of Macroporous Lead-Free Piezoelectric Ba0. 85Ca0. 15Zr0. 1Ti0. 9O3," J. Am. Ceram. Soc., **102**(6), pp. 3191–3203.
[32] Zhou, N., Liu, C., Lewis, J. A., and Ham, D., 2017, "Gigahertz Electromagnetic Structures Via Direct Ink Writing for Radio-Frequency Oscillator and Transmitter Applications," Adv. Mater., **29**(15), p. 1605198.
[33] Sheng, Y., Jiang, N., Lu, S., Zhao, Y., Wang, Q., Ma, L., and Liu, X., 2019, "Molecular Interaction and Foaming Property of the Mixtures of Hydrocarbon, Fluorocarbon and Silicone Surfactants," J. Mol. Liq., **296**, p. 111836.
[34] Liu, Q., Liu, S., Luo, D., and Peng, B., 2019, "Ultra-Low Interfacial Tension Foam System for Enhanced Oil Recovery," Appl. Sci., **9**(10), p. 2155.
[35] Sengupta, R., Khair, A. S., and Walker, L. M., 2020, "Dynamic Interfacial Tension Measurement Under Electric Fields Allows Detection of Charge Carriers in Nonpolar Liquids," J. Colloid Interface Sci., **567**, pp. 18–27.